Journal of Medicinal Chemistry

ARTICLE

pubs.acs.org/jmc

Identification of the Binding Modes of *N*-Phenylphthalimides Inhibiting Bacterial Thymidylate Synthase through X-Ray Crystallography Screening

Stefano Mangani,[*,‡] Laura Cancian,[†] Rosalida Leone,[‡,§] Cecilia Pozzi,[‡] Sandra Lazzari,[†] Rosaria Luciani,[†] Stefania Ferrari,[*,†] and M. Paola Costi[*,†]

[†]Dipartimento di Scienze Farmaceutiche, Università degli Studi di Modena e Reggio Emilia, Via Campi 183, 41126 Modena, Italy

[‡]Dipartimento di Chimica, Università degli Studi di Siena, Via Aldo Moro 2, 53100 Siena, Italy

Supporting Information

ABSTRACT: To identify specific bacterial thymidylate synthase (TS) inhibitors, we exploited phenolphthalein (PTH), which inhibits both bacterial and human enzymes. The X-ray crystal structure of *Lactobacillus casei* TS (LcTS) that binds PTH showed multiple binding modes of the inhibitor, which prevented a classical structure-based drug design approach. To overcome this issue, we synthesized two phthalimidic libraries that were tested against TS enzymes and then we performed X-ray crystallographic screening of the active compounds. Compounds **6A**, **8A**, and **12A** showed 40-fold higher affinity for bacterial TS than human TS. The X-ray crystallographic screening characterized the binding mode of six inhibitors in complexes with LcTS. Of these, **20A**, **23A**, and **24A** showed a common unique binding mode, whereas **8A** showed a different, unique binding mode. A comparative analysis of the LcTS X-ray complexes that were obtained with the pathogenic TS enabled the selection of compounds **8A** and **23A** as specific compounds and starting points to be exploited for the specific inhibition of pathogen enzymes.

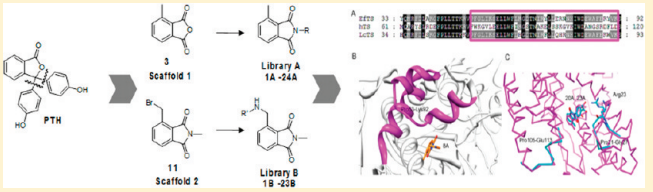

INTRODUCTION

Thymidylate synthase (TS) (EC 2.1.1.45) catalyzes the reductive methylation of 2′-deoxyuridine-5′-monophosphate (dUMP) to form 2′-deoxythymidine-5′-monophosphate (dTMP), using the cofactor N^5,N^{10}-methylene tetrahydrofolate (MTHF). Because TS represents the only means of synthesizing dTMP in human cells and in many pathogens, it is typically a target in designing chemotherapeutic agents such as anticancer drugs and, more recently, antibacterial drugs.[1−10]

In previous work, we obtained three X-ray crystal structures of *Lactobacillus casei* TS (LcTS) in a complex with phenolphthalein (PTH)[3,4] or naphthalein derivatives (α156, PDB ID 1TSL; MR20, PDB ID 1TSM) and one X-ray crystal structure of *Escherichia coli* TS (EcTS) in complex with a naphthalein derivative (GA9, PDB ID 2A9W)[5,9] (Supporting Information, Figure S1). Those results showed that when ligands of this class of compound entered into the active site, they adopted multiple binding modes; therefore, it was not possible to identify the key interactions made by the compounds within the binding site. Consequently, structure-based drug design is difficult to perform and the results might be inconclusive.

To develop high-affinity inhibitors targeting bacterial TS, we needed to identify specific inhibitors that presented a unique binding mode. Therefore, starting from PTH, we designed and synthesized a new class of phthalimidic compounds using a ligand-based approach with two scaffolds. The first round of synthesis provided specific compounds with moderate affinity for bacterial TS. X-ray crystallographic screening of the compound library yielded four crystallographic LcTS−inhibitor complexes showing unique binding modes. Information gained through the crystallographic studies on LcTS suggests structural guidelines that would prospectively lead to more specific, higher-affinity inhibitors toward TS from pathogenic organisms.

RESULTS AND DISCUSSION

Scaffold Identification and Validation. PTH has received little attention as a TS inhibitor, with the exception of a limited structure−activity relationship study that investigated phenol-substituted analogues.[7,8,10] We further explored PTH through a retrosynthetic approach[11] to identify fragments that could be further elaborated (Figure 1). Two fragments were identified: phenol (**1**) and 2-benzofuran-1,3-dione (**2**). The phenol was not considered useful because of its small size and its expected low binding specificity. By contrast, the 2-benzofuran-1,3-dione was more suitable for multiple derivatizations; therefore, we used this core structure to examine the ChemFinder database.[12] A number of compounds were retrieved, and we identified eight potential scaffolds, compounds **2**−**9** (Figure 2), for further synthetic

Received: April 25, 2011
Published: June 22, 2011

elaboration. In a preliminary chemical modification study, we applied different synthetic strategies. Compounds **3** (4-methyl-2-benzofuran-1,3-dione) and **4** (5-methyl-2-benzofuran-1,3-dione) were the most promising molecules because, with an amine library, we could selectively derivatize either the phthalic oxygen and/or positions 4 or 5, with a preliminary bromination. With respect to the bromination of the methyl group, compound **3** was the most active and compound **4** did not react properly. Compound **3** was selected as scaffold 1 for the subsequent production of the substituted phthalimide libraries. A second scaffold was derived from compound **3**, where the anhydride functionality was aminomethylated and the methyl in position 4 was modified to a bromo-methylene group to obtain scaffold 2 (i.e., compound **11**) (Scheme 1).

Design and Synthesis of Libraries A and B. A fragment virtual library based on molecular diversity was designed with ChemFinder software.[12] Of the 23130 available amines, we discarded molecules (fragments) with a molecular weight greater than 200 Da, those that were structurally complex, and those with cross-reacting groups. The remaining 303 molecules were further filtered. Their molecular properties were calculated (ACD Laboratories 6.0),[13] and the final number was reduced to 47 candidates according to Lipinsky's rules,[14] molecular diversity, and commercial availability.

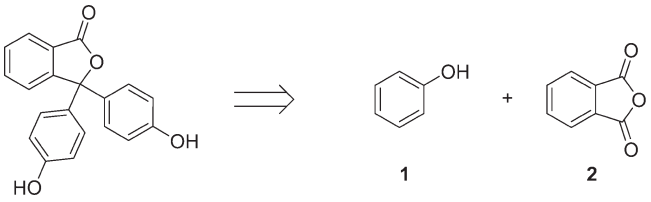

Figure 1. Retrosynthetic analysis of phenolphthalein (PTH).

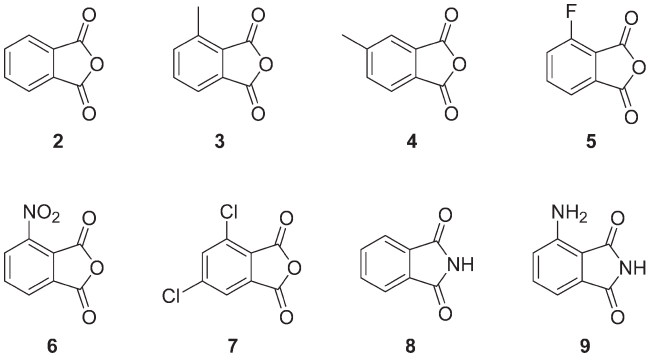

Figure 2. Compounds **2**−**9** were identified for further synthetic elaboration through ChemFinder database exploration based on 2-benzofuran-1,3-dione (**2**).

The fragments used to synthesize libraries A and B were chosen to ensure that all the expected compounds possessed satisfactory drug-like properties and high molecular diversity (Supporting Information Charts S1 and S2, Table S1, Figure S2). The compounds of library A possessed molecular masses ranging from 238 to 451 Da, exhibited predicted water solubility between 3.6×10^{-7} and 1.34 mol/L, and had computed octanol/water partition coefficients (clogD values) from −2.21 to 5.52 (pH 7.4). The compounds of library B had molecular masses ranging from 243 to 370 Da, had predicted water solubilities from 2.6×10^{-6} to 0.14 mol/L, and displayed clogD values from −3.80 to 4.46 (pH 7.4).

Library A derivatives were prepared with two different methods. In method 1, a small excess of the appropriate amine, previously dissolved in ethanol, was added dropwise to a solution of scaffold 1 in toluene, and the reaction mixture was refluxed for 15 h. The solvent was removed under reduced pressure, and the residue was washed with ethanol to eliminate excess amine. In method 2, the opportune amine and scaffold 1 were mixed at an equimolar ratio in acetic acid, and then the reaction mixture was refluxed for 5 h. After precipitation with water, the product was isolated by filtration. Compounds **1A**, **4A**, **6A**, **11A**−**12A**, **15A**, **18A**−**19A**, and **21A**−**23A** were synthesized using method 1, and compounds **5A**, **8A**, **17A**, **20A**, and **24A** were synthesized using method 2. The synthesis of library B commenced with the bromination of 2,4-dimethyl-1*H*-isoindole-1,3(2*H*)-dione (**10**) with *N*-bromosuccinimide and benzoyl peroxide under UV light to produce a good yield of 4-(bromomethyl)-2-methyl-1*H*-isoindole-1,3(2*H*)-dione (**11**). Treatment of **11** with the suitable amine in DMF at 75 °C for 15 h produced compounds **3B**, **4B**, **7B**, **9B**, **11B**, **13B**, **15B**, **16B**, **22B**, and **23B**. A total of 26 compounds were obtained with at least 95% purity.

Biological Evaluation of Libraries A and B. The 26 synthesized compounds were tested against TS enzyme from humans,

Scheme 1[a]

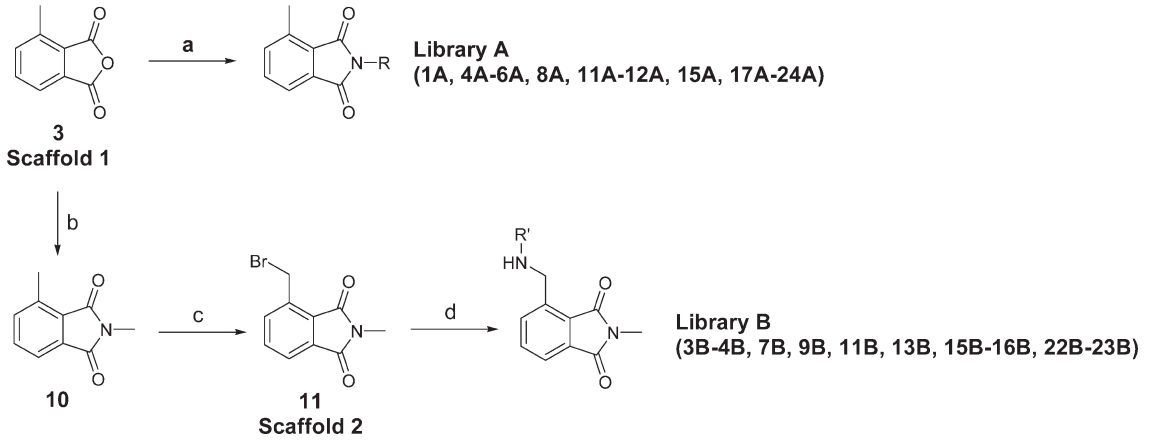

[a] Reagents and conditions: (a) method 1: the opportune amine, toluene, EtOH, reflux, 15 h; method 2: the opportune amine, acetic acid, reflux, 5 h. (b) NH_2CH_3, toluene, EtOH, yield 47%; (c) NBS, benzoyl peroxide, CCl_4, hν, yield 64%; (d) the opportune amine, DMF, 75 °C, 15 h.

dx.doi.org/10.1021/jm2005018 |*J. Med. Chem.* 2011, 54, 5454–5467

Table 1. Biological Activity of Libraries A and B Derivatives[a]

code	K_i hTS[b]	K_i EcTS[b]	K_i EfTS[b]	K_i LcTS[b]
α156[c]	30 ± 5	0.60 ± 0.12		0.70 ± 0.15
PTH[d]	1.2 ± 0.2		1.4 ± 0.3	4.7 ± 0.9
3 (scaffold 1)	ni	49 ± 10	ni	ni
11 (scaffold 2)	ni	ni	ni	95 ± 22
1A	ni	ni	ni	20 ± 4
4A	ni	ni	ni	44 ± 6
5A	ni	18 ± 2	60 ± 12	14 ± 2
6A	ni	111 ± 25	7.0 ± 1.4	23 ± 5
8A	ni	31 ± 6	8.0 ± 1.6	22 ± 5
11A	206 ± 41	ni	33 ± 7	34 ± 7
12A	81 ± 16	3.0 ± 0.6	2.0 ± 0.35	3.0 ± 0.6
15A	ni	ni	11 ± 2	ni
17A	60 ± 12	42 ± 8	11 ± 2	ni
18A	ni	ni	61 ± 17	93 ± 19
19A	30 ± 6	ni	ni	69 ± 14
20A	43 ± 9	36 ± 7	ni	14 ± 4
21A	ni	ni	26 ± 5	25 ± 5
22A	ni	33 ± 7	ni	36 ± 7
23A	ni	41 ± 8	ni	6.0 ± 1.2
24A	ni	ni	ni	9.0 ± 1.6
3B	ni	ni	ni	27 ± 5
4B	ni	ni	109 ± 22	56 ± 11
7B	48 ± 10	ni	183 ± 37	41 ± 8
9B	ni	61 ± 12	ni	ni
11B	21 ± 4	42 ± 8	ni	33 ± 7
13B	ni	82 ± 16	ni	14 ± 3
15B	ni	ni	ni	51 ± 10
16B	ni	92 ± 18	ni	10 ± 2
22B	ni	14 ± 3	ni	ni
23B	ni	ni	ni	38 ± 8

[a] K_i for the enzymes tested are reported (K_i hTS, K_i EcTS, K_i LcTS, K_i LcTS). [b] ni = no detectable inhibition at 50 μM. [c] Already reported in refs 1,2, and 6. [d] Already reported in ref 5.

from the pathogenic bacteria *Escherichia coli* and *Entercoccus faecalis*, and from the model bacteria *Lactobacillus casei* with a rapid screening assay (Table 1 and Supporting Information Figure S3). All active compounds showed competitive inhibition with respect to the MTHF cofactor.

Compound **3** was tested against TS enzymes and showed moderate affinity for EcTS (20% inhibition at 50 μM) but did not show affinity for human TS (hTS) (no activity at 50 μM).

Compounds **11A**, **17A**, **19A**, and **20A** that inhibited hTS were deemed less likely candidates than those such as **5A**, **6A**, **8A**, **15A**, and **21A** that had no activity against hTS but had K_i values below 30 μM for EcTS or *Entercoccus faecalis* TS (EfTS). Compound **12A** had activity against hTS but even greater activity against EcTS and EfTS, so the compound displayed selectivity.

Within library B, only one compound (**22B**) inhibited EcTS with a K_i value lower than 30 μM; none of the compounds show K_i values lower than 30 μM against EfTS. Only two compounds, **7B** and **11B**, showed some inhibitory activity against hTS with K_i values of 48 and 21 μM, respectively. All the other candidates in library B showed no detectable inhibitory activity against hTS at 50 μM concentration.

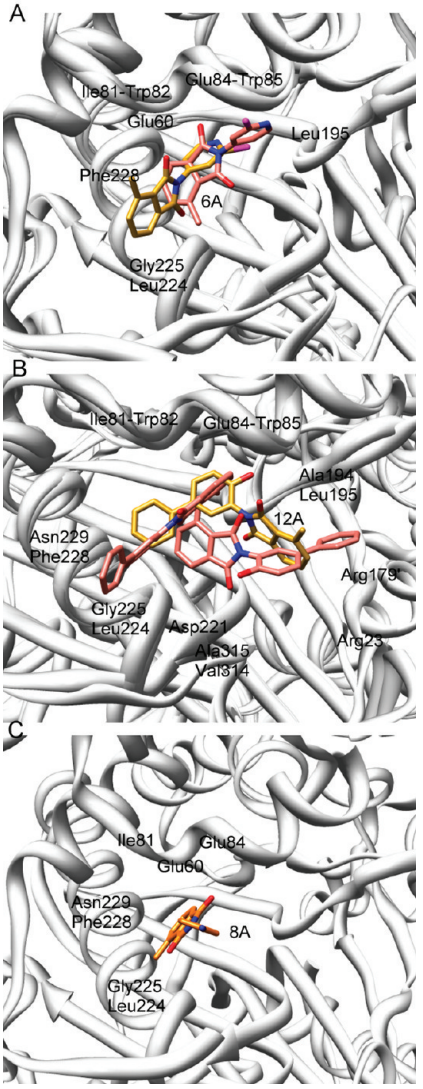

Figure 3. (A) Superposition of the two crystal structures of LcTS-dUMP−**6A**. (B) Superimposition of the two crystal structures of LcTS-dUMP−**12A**. Compound **12A** was modeled in two possible bound conformations in one crystal structure (PDB ID 3BYX; the two conformations are shown with C in pink in the picture). (C) Crystal structure of LcTS-dUMP−**8A**. The protein is represented as a ribbon; ligands are represented as sticks that are color-coded according to the atom (N in blue, O in red, C in pink, yellow, or orange).

All compounds were also tested against LcTS because it is often used in TS crystallographic studies, even though it is from a nonpathogenic bacteria. All but four of the compounds (**15A**, **17A**, **9B**, and **22B**) were active against LcTS, with K_i values ranging from 3 to 93 μM.

X-Ray Crystallographic Screening. We performed X-ray crystallographic screening to gain the necessary structural information on the binding modes of these compounds. Compared to library B, library A had a higher number of and more active and specific compounds that were easier to synthesize. Nevertheless, our attempts to crystallize library A compounds in complex with TS from the different pathogens (EcTS and EfTS) failed; crystal structures were obtained only with a TS from a nonpathogenic bacteria, LcTS. Despite not being able to rule out that the same compounds could show different binding modes in other bacterial

dx.doi.org/10.1021/jm2005018 |*J. Med. Chem.* 2011, 54, 5454–5467

Table 2. Data Collection and Refinement Statistics for X-Ray Structures of Compounds 6A, 8A, 12A, 20A, 23A, and 24A Bound to *Lactobacillus casei* Thymidylate Synthase (LcTS) and its Substrate, 2′-Deoxyuridine-5′-monophosphate (dUMP)

	LcTS-dUMP–**6A**_1 3C06	LcTS-dUMP–**6A**_2 3C0A	LcTS-dUMP–**8A** 3BNZ	LcTS-dUMP–**12A**_1 3BYX	LcTS-dUMP–**12A**_2 3BZ0	LcTS-dUMP–**20A** 3IK1	LcTS-dUMP–**23A** 3IJZ	LcTS-dUMP–**24A** 3IK0
beamline	ESRF ID14−1	ESRF ID23−1	ESRF ID14−1	ESRF ID14−1	EMBL BW7B	ESRF ID23−1	ESRF ID23−1	ESRF ID23−1
data collection oscillation angle (deg)	1	0.75	1	1	1	0.5	0.5	0.5
wavelength, (Å)	0.930	1.008	0.930	0.930	1.078	0.983	0.983	0.983
space group	$P6_122$	$P6_122$	$P6_122$	$P6_122$	$P6_122$	$P6_122$	$P6_122$	$P6_122$
cell dimensions (Å)	a = 76.57	a = 78.52	a = 76.56	a = 77.01	a = 77.92	a = 77.99	a = 77.66	a = 78.20
	b = 76.57	b = 78.52	b = 76.56	b = 77.01	b = 77.92	b = 77.99	b = 77.66	b = 78.20
	c = 212.93	c = 224.38	c = 213.07	c = 213.97	c = 224.18	c = 224.72	c = 224.97	c = 226.66
Z	12	12	12	12	12	12	12	12
resolution (Å)	38.29−2.60	50.12−2.40	36.04−2.60	48.74−2.40	33.40−2.70	67.57−2.25	66.27−2.21	75.59−2.10
total refln	95318	171356	49201	71236	41655	401629	341948	430226
unique refln	11312	16592	11909	13070	10443	20159	20713	24941
completeness (%)	98.2	98.4	98.4	84.4	88.6	99.9	98.2	99.9
R_{sym} (%)	0.100	0.095	0.169	0.095	0.139	0.079	0.093	0.106
multiplicity	8.4	10.3	4.1	5.4	4.0	19.9	16.5	17.2
$I/\sigma(I)$	6.4	5.6	2.7	7.0	4.3	37.7	29.6	27.7
R_{cryst} (%)	21.86	25.54	21.42	20.83	22.58	21.5	21.0	20.9
R_{free} (%)	29.18	32.61	32.31	28.32	32.62	27.1	25.3	25.8
protein atoms	2507	2394	2566	2577	2521	2762	2754	2786
ligands	39	39	45	70	45	41	40	40
water molecules	40	78	73	123	36	158	146	178
Ramachandran plot stats (%)								
most allowed	81.8	88.5	87.8	90.8	81.6	93.5	94.5	96.1
allowed	18.2	11.5	12.2	9.2	18.0	6.5	5.5	3.9
gen allowed					0.4			
rmsd bond lengths (Å)	0.02	0.02	0.02	0.01	0.02	0.02	0.02	0.02
rmsd bond angles (deg)	2.11	2.20	2.17	1.93	2.15	2.03	2.23	1.84

dx.doi.org/10.1021/jm2005018 |*J. Med. Chem.* 2011, 54, 5454–5467

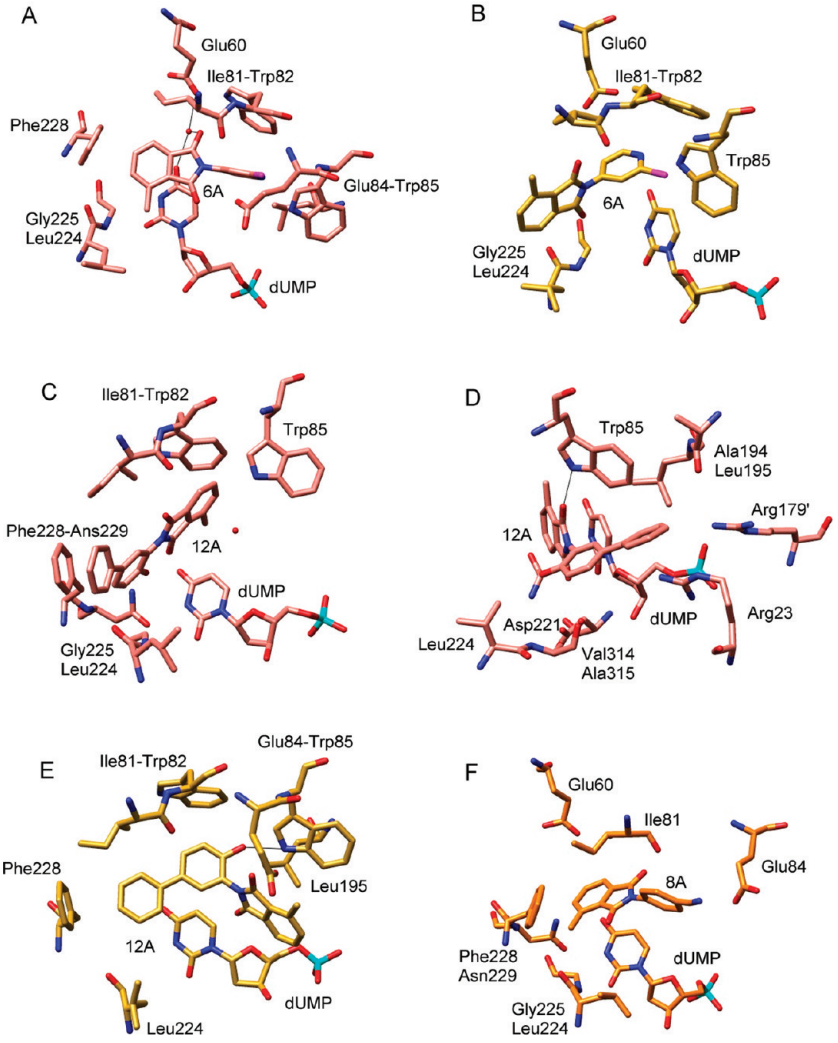

Figure 4. Binding modes of compounds as observed in the crystal structures. (A) **6A** bound in crystal structure 3C0A or (B) in crystal structure 3C06. (C and D) Compound **12A** is shown in its (C) first binding mode and (D) second binding mode as modeled in crystal structure 3BYX. (E) Compound **12A** is shown in its binding mode in the 3BZ0 crystal structure; (F) compound **8A** bound in the 3BNZ crystal structure.

enzymes, we could use proven binding modes as a guide to design better derivatives taking into account the structural differences among the different enzymes.

Eight crystals of LcTS bound to six different ligands (**6A**, **8A**, **12A**, **20A**, **23A**, and **24A**) were successfully obtained and analyzed (Table 2). The LcTS structure consisted of a homodimer with the two subunits related by a 2-fold crystallographic axis of the hexagonal $P6_122$ space group; all LcTS-complex crystals showed this symmetry. Each LcTS subunit had two domains. The larger domain (residues 1−69 and 141−316) had an α/β structure with six α-helices, one β-hairpin, a two-stranded β-sheet, and a five-stranded β-sheet. The second domain, termed the small domain (SD, residues 70−139), consisted of four α-helices and a long interconnecting loop.[15] This region consistently showed low electron density as a result of structural flexibility, especially between residues 95 and 120, which could not be modeled in some of the structures. The active site cavity was embedded in the large domain, but one of its walls contained two Arg residues (Arg178′ and Arg179′) from the symmetry-related subunit; these Arg residues contributed to the binding site of the dUMP phosphate moiety. The active site residues involved in catalysis included the nucleophilic Cys198, Ser219, His259, and Asn229, which could interact with the dUMP ribose and uridine moieties, as well as Ile81, Trp82, Trp85, Leu224, Phe228, and Val314, which defined a large hydrophobic cavity capable of hosting the aromatic moiety of MTHF. After the determination and refinement of the crystal structure (see Experimental Section), the $F_o - F_c$ difference Fourier maps (ΔF) were calculated with phases from the refined LcTS model; these ΔF maps were inspected to identify the bound inhibitor molecule. The ΔF maps showed a large positive electron density (between 2σ and 7σ) in the active sites due to the presence of dUMP and the different ligands. Although the ΔF maps showed a low or incomplete electron density for the inhibitor molecule, we were able to confidently position the main features of the ligand molecules. The dUMP substrate occupied the usual dUMP site, which extended from the phosphate binding site (Arg23, Arg218, and Ser219 from one subunit and Arg178′ and Arg179′ from the symmetry-related subunit), located at the interface between the two subunits, to the pyrimidine binding site located deeper in the cavity between the backbone of Asp221 and the side chain of Asn229.[16]

dx.doi.org/10.1021/jm2005018 |*J. Med. Chem.* 2011, 54, 5454–5467

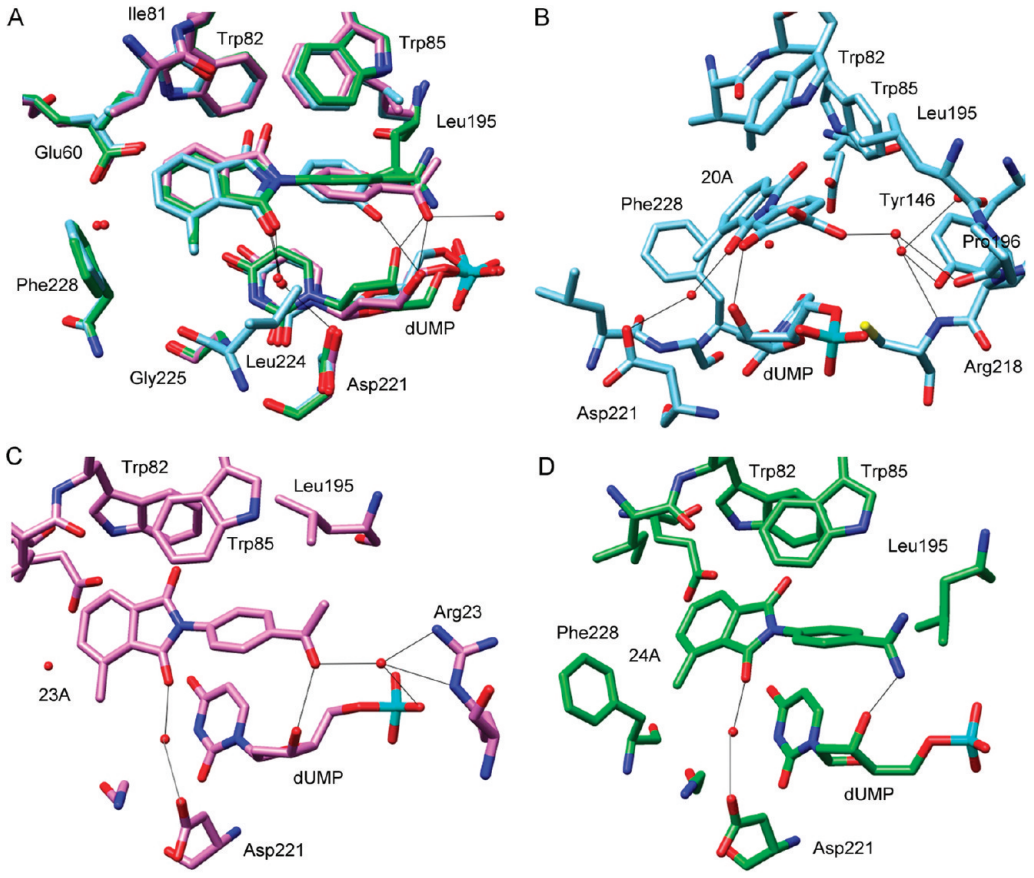

Figure 5. (A) Superposition of the crystal structures for LcTS-dUMP−**20A**, LcTS-dUMP−**23A**, and LcTS-dUMP−**24A**. (B) Detailed interactions of the phenyl moiety of ligand **20A** with LcTS. (C) Detailed interaction of the phenyl moiety of ligand **23A** with LcTS. (D) Detailed interaction of the phenyl moiety of ligand **24A** with LcTS. All structures are color-coordinated, with oxygen in red, nitrogen in blue, sulfur in yellow, and phosphate in cyan. Carbon atoms are sky blue, purple, and green in LcTS-dUMP−**20A**, LcTS-dUMP−**23A**, and LcTS-dUMP−**24A**, respectively. Hydrogen bonds are indicated with black lines.

For two ligands (**6A** and **12A**; parts A and B of Figure 3, respectively), the X-ray crystallographic screen was used to identify different binding modes. For each ligand, two structures were obtained from independent crystallization and diffraction experiments that showed the molecule bound in distinct orientations to the active site of LcTS. In one crystal structure (PDB ID C03A), the inhibitor **6A** formed stacking interactions with Phe228, Trp82, and Trp85, a hydrogen bond with Glu60, and contact interactions with Ile81, Glu84, Leu195, Leu224, and Gly225 (Figure 4A). In the other crystal structure (PDB ID 3C06), **6A** formed stacking interactions with Trp82, Trp85, and the pyrimidine ring of dUMP as well as contact interactions with Ile81, Leu224, and Gly225 (Figure 4B). A comparison of the two structures showed that, in 3C0A, the phthalimidic ring of **6A** was rotated by ~90° with respect to its position in 3C06 (Figure 3A). The observed binding modes of **6A** in the two complexes displayed three important features: (i) the **6A** pyridine ring was located close to Trp82 and Trp85, (ii) the chlorine (Cl) atom interacted with the indole Nε1 atom of Trp85, and (iii) the phthalimidic moiety of **6A** was involved in the aromatic stacking interactions with dUMP or with Phe228.

In the case of compound **12A**, one structure (PDB ID 3BZ0), even though it was viewed at a relatively low resolution (2.70 Å), allowed us to model the ligand at full occupancy. By contrast, the other structure (PDB ID 3BYX; resolution 2.40 Å) had a weaker electron density; thus, the ligand was modeled in two possible bound conformations, and partial occupancy was assigned to each conformation (Figure 4C, 4D). In the first binding mode observed for molecule **12A** (PDB ID 3BYX, conformation A), no hydrogen bond was formed, but stacking interactions were observed with Phe228 and Trp82 and contacts were made with Ile81, Trp85, Leu224, Gly225, Asn229, and dUMP (Figure 4C). In the second binding mode observed for molecule **12A** (PDB ID 3BYX, conformation B), a hydrogen bond was formed with Trp85, stacking interactions were made with Trp85 and dUMP, and contact interactions were made with Arg23, Ala194, Leu195, Asp221, Gly225, Val314, Ala315, and Arg179′ (Figure 4D). In the last binding mode observed for molecule **12A** (PDB ID 3BZ0), a hydrogen bond was formed with Trp85, stacking interactions were made with Trp82, Trp85, Phe228, and dUMP, and contact interactions were made with Ile81, Glu84, Leu195, and Leu224 (Figure 4E).

Compounds **6A** and **12A** show the best outcome from this study based on having the best affinity and specificity profiles; however, their multiple binding modes prevent the possibility of applying a structure-based approach for further structural development.

In the case of the LcTS-dUMP−**8A** complex (PDB ID 3BNZ), the ΔF map showed positive electron density in the active site that was clearly attributable to dUMP. Less density was present in the hydrophobic pocket, where the inhibitor was

dx.doi.org/10.1021/jm2005018 |*J. Med. Chem.* 2011, 54, 5454–5467

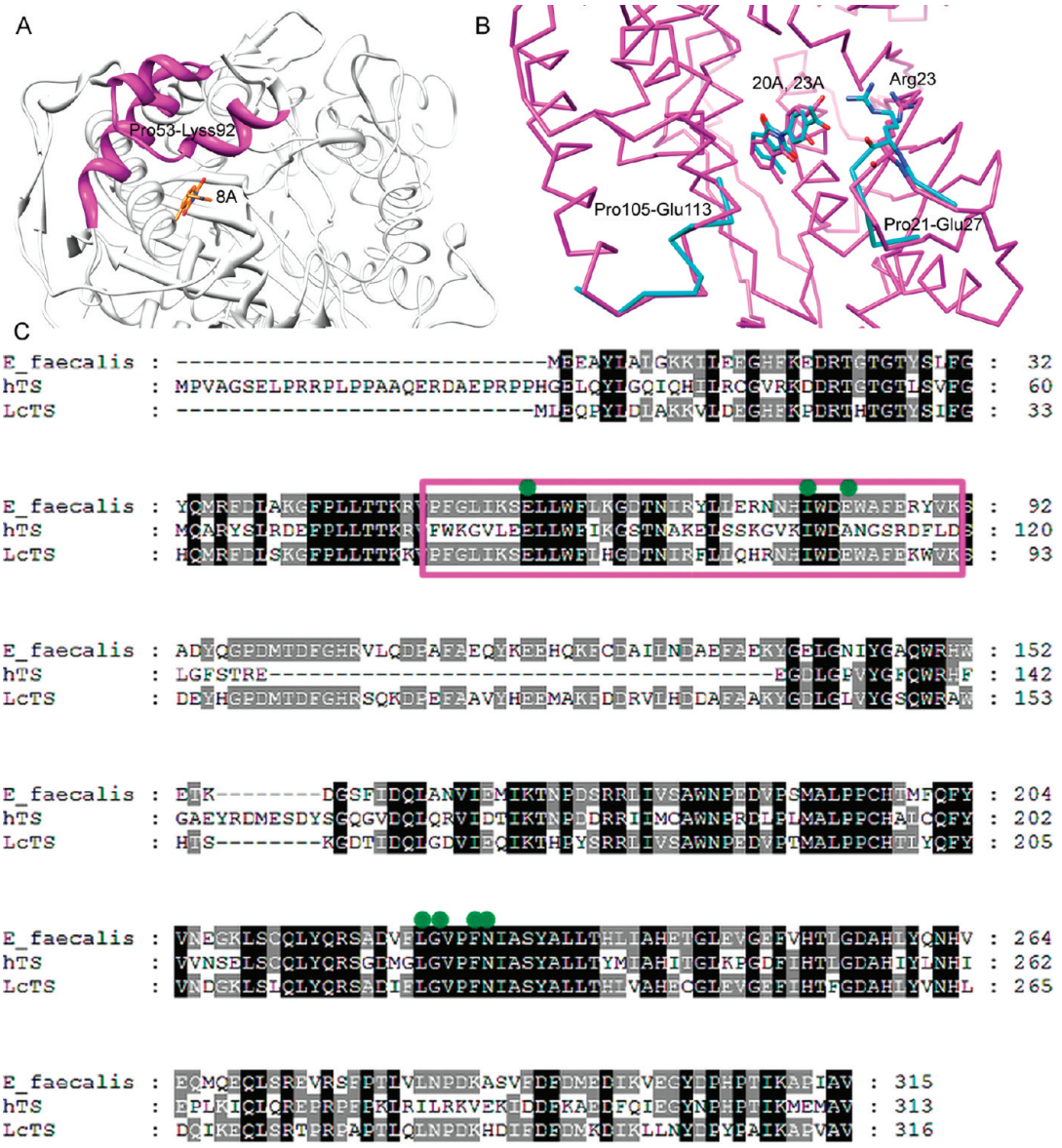

Figure 6. (A) Details of the LcTS−**8A** complex. Colored in magenta is the Pro53-Lys92 sequence. (B) Structure comparison of LcTS−**20A** (in magenta) and LcTS−**23A** (in cyan) complexes. For clarity purposes, only Arg23 residue and Pro21-Gly27 and Pro105-Glu113 trace sequences of LcTS−**23A** complex are shown to highlight the conformational differences between these two complexes. (C) Protein sequence alignment of EfTS, hTS and LcTS; written in white on a black background are identical residues among the three sequences; written in white on a gray background are identical residues between two out of three sequences. The magenta rectangle highlights the sequence Pro53-Lys92 (LcTS sequences number) that is more conserved between the two bacterial TS with respect to hTS; the green circles indicate the residues interacting with compound **8A**.

expected to bind. Compound **8A** interacted with LcTS by forming stacking interactions with Phe228 and dUMP and by making contacts with Glu60, Ile81, Glu84, Leu224, Gly225, and Asn229 (Figure 3C). Thus compound **8A** with its single binding mode represents a good initial candidate for EfTS inhibition. However, the EfTS crystallographic structure is not available in the Protein Data Bank for a three-dimensional comparison of the different TS isoforms. Sequence alignment (Figure 6C) showed that all the residues interacting with compound **8A** are conserved between LcTS and EfTS. Comparison with hTS showed that of these residues, only Glu84 is not conserved (Ala in hTS); the whole sequence (Pro53-Glu88) surrounding the interacting residues forming the side wall of the **8A** binding site is more conserved between LcTS and EfTS on one side than between LcTS and hTS on the other side (Figure 6A, 6C). These differences could account for the observed specificity.

Three ligands (**20A**, **23A**, and **24A**) showed a common binding pattern, where the phthalimidic core of these molecules formed (i) stacking interactions with Trp82, Phe228, and the pyrimidine ring of the substrate, dUMP, (ii) a hydrogen bond with Asp221 through a conserved water molecule, and (iii) contacts with Glu60, Ile81, Leu224, and Gly225 (Figure 5A). In all cases, because of the substituent linked at the phthalimidic nitrogen, the phenyl ring on the substituent interacted with the uridine ring of dUMP, with Trp85 (stacking interactions) and with Leu195 (contact). Small differences were observed in the hydrogen-bonding network due to the different functional groups that were present on the phenyl ring. In the case of **20A**, the

dx.doi.org/10.1021/jm2005018 |*J. Med. Chem.* 2011, 54, 5454–5467

Chart 1. Library A, Compounds 1A−24A

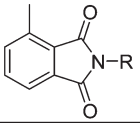

Code	Structure of R	Code	Structure of R	Code	Structure of R
1A	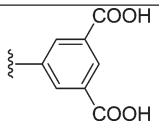	4A	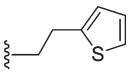	5A	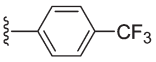
6A	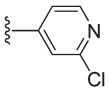	8A	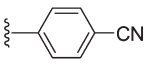	11A	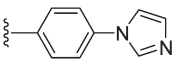
12A	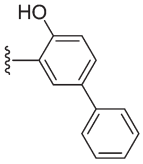	15A		17A	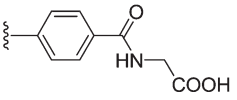
18A	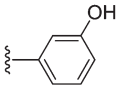	19A	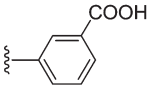	20A	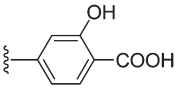
21A	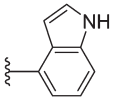	22A	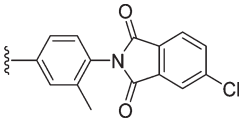	23A	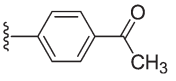
24A	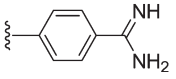				

hydroxyl group established a hydrogen bond with the ribose ring of dUMP, and the carboxyl group formed hydrogen bonds mediated by 1 or 2 water molecules with Tyr146, Pro196, and Arg218 (Figure 5B). In the case of compound **23A**, the acetyl group interacted with the ribose moiety of dUMP through a water molecule bridge, with the phosphate moiety of dUMP and with Arg23 (Figure 5C). In compound **24A**, the amidine group formed only a hydrogen bond with the ribose moiety of dUMP (Figure 5D).

Initially, we obtained compounds that showed unique binding modes to LcTS, such as **8A**, **20A**, **23A**, and **24A**. This is the first time that inhibitors structurally unrelated to the folate cofactor crystallized with the TS protein in a unique binding mode. However, it was necessary to understand how to use the information obtained on a nonpathogenic TS, such as LcTS, to design effective antibacterial agents against EcTS and EfTS targets. With this aim, we critically analyzed each crystallographic complex and then selected the most suitable complexes for further studies.

Compounds **20A**, **23A**, and **24A** showed different specificity profiles: **20A** is active toward LcTS, EcTS, and hTS, and thus, it is not specific; **23A** is active toward LcTS and EcTS, and thus, it is moderately specific; **24A** is active only toward LcTS, and thus, it is of low interest. Comparison of LcTS−**20A** and LcTS−**23A** complexes shows that among the residues interacting with the two ligands, there is a conformational change in residue Arg23. This residue moves toward the ligand in the case of **23A** (Figure 6B). Analyzing the whole protein trace reveals that conformational changes between the two structures involve the whole sequence (Pro21-Gly27) as well as the adjacent small domain sequence from Gly105 to Glu113 (Figure 6B). Previous computational studies[17,18] described how these two regions move in a coordinated manner during the flexibile motion of the protein highlighting major differences between bacterial TS and hTS. We suggest that the differences in the dynamics of LcTS vs hTS could be fundamental to the specific profile of compound **23A**.

Structure-Based−Activity Relationships. All eight structures showed that all the ligands bound in the active site of the enzyme where the MTHF cofactor and the classical folate analogue inhibitors usually bind. This accounted for the competitive inhibition observed in the enzyme inhibition assays, in which competition for binding with the folate substrate was observed. Although all these compounds (**6A**, **8A**, **12A**, **20A**, **23A**, and **24A**) could bind to the same site, they showed different binding modes depending on the substituent present on the phthalimidic nitrogen; the phthalimidic core contributed to the interaction with the enzyme, but this core alone was unable to recognize a specific binding site in the enzyme active site cavity (Chart 1).

Three pairs of compounds from the two libraries have the same or similar substituents R/R′ (R on position 2 of scaffold 1 and R′ on position 4 of scaffold 2): **4A**−**9B**, **8A**−**15B**, and **23A**−**4B**. The compounds within the first pair show different specificity profiles. Compound **4A** is active only toward LcTS (K_i = 44 μM), while **9B** is inactive against LcTS and active only toward EcTS (K_i = 61 μM); no structural data was obtained with these compounds. In the pair **8A**−**15B**, compound **8A** is active toward all the bacterial enzymes, while compound **15B** is active

dx.doi.org/10.1021/jm2005018 |*J. Med. Chem.* 2011, 54, 5454–5467

Chart 2. Library B, Compounds 1B−23B

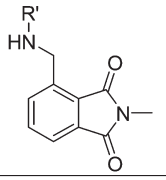

Code	Structure of R'	Code	Structure of R'	Code	Structure of R'
3B	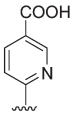	4B	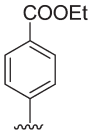	7B	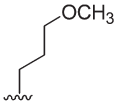
9B	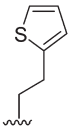	11B	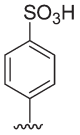	13B	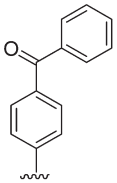
15B	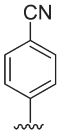	16B	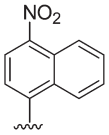	22B	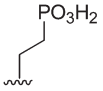
23B	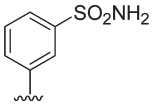				

only against LcTS. The analysis of the crystallographic complex of LcTS and **8A** (K_i of 22 μM) suggested that the binding site of **8A** can be conserved also for **15B** (K_i of 51 μM); **15B** can bind with slight motion of the enzyme to accommodate the larger R′ group in position 4 of scaffold 2 (Chart 2). Considering the case in which the main stacking interaction with Phe228 and dUMP are conserved, the **15B** ligand could, by flipping around the pthalimidic plane with respect to **8A**, cause its larger substituent in position 4 to interact with Trp82 and Phe64. Both compounds **23A**−**4B**, in which the two substituents are quite similar, show that they are both inactive toward hTS and active toward LcTS, even if **4B** is approximately 10 times less active than **23A** (6 and 56 μM, respectively); however, they differ in the activity toward the other bacterial enzymes: **23A** is active toward EcTS, while **4B** is active toward EfTS. The analysis of the crystallographic complex of LcTS and **23A** suggested that the binding site of **23A** can be conserved also in the case of **4B**, with a slight rotation of the ligand to accommodate the bigger R′ group in position 4 of scaffold 2. In this way it is possible that the main stacking interaction with Trp82 and Phe228 are retained and that this larger R′ substituent could face the inner pocket of the active site (particularly toward Phe64 and Tyr146) or toward the outer pocket.

CONCLUSION

In searching for new specific inhibitors of bacterial TS enzymes, we combined a ligand-based design study and a X-ray crystallographic screening of the synthesized libraries to characterize the binding modes of the active compounds.

From PTH, a lead inhibitor unsuitable for structure-based drug design, we derived two potential scaffolds that we then used to design and synthesize candidate compound libraries. Derivatization of scaffold 1 gave active compounds in library A, which could be further crystallized with LcTS. The best compounds from this new series had K_i values in the same range as that of PTH toward bacterial TS but they showed lower or no activity against human TS, therefore they are selective for the pathogenic enzymes. X-ray crystallographic screening was applied and provided eight structures of LcTS complex with six compounds out of 26 compounds analyzed. Only compounds **20A**, **23A**, and **24A**, revealed a unique binding mode and a common binding pattern as shown by the crystallographic complexes, while compound **8A** showed a different but unique mode of binding. Even if our study was limited by having crystal structures from a non pathogenic TS, i.e. LcTS, it demonstrates that the suggested approach can successfully characterize the binding mode of the library compounds and identify unique binding modes even in cases of such a large and hydrophobic active site as that of TS.

In conclusion, our library design and subsequent crystallographic screening represent a strategic tool for providing leads with unique binding modes which are thus suitable starting points for further medicinal chemistry elaboration. In our case, further studies will take advantage of information derived from crystallographic analysis on compounds **8A** and **23A** to address the structure-based optimization of the phthalimidic core to develop other derivatives that retain their binding profile but have improved activity and specificity.

EXPERIMENTAL SECTION

Synthesis and Characterization of Libraries A and B. Reactions were performed using Büchi's Syncore parallel synthesizer, which allowed the simultaneous production of 24 reactions. Reaction

dx.doi.org/10.1021/jm2005018 |J. Med. Chem. 2011, 54, 5454–5467

progresses were monitored by TLC on precoated silica gel 60 F_{254} plates (Fluka), and visualization was accomplished with UV light (254 nm). The purity of all synthesized compounds was determined by elemental analyses performed on a Perkin-Elmer 240C instrument, and the results were within ±0.4% of the theoretical values. All the compounds tested through a rapid screening assay show >95% purity. Yields of these reactions referred to purified products, and not optimized, were: compounds A method 1 in the range of 20−50%, method 2 in the range 35−55% (except **24A** and **8A**, whose yields were 13% and 73% respectively), compounds B method 3 in the range 20−45%. Melting points were determined on a Stuart SMP3 capillary melting point apparatus and are uncorrected. All compounds were characterized by ^{1}H NMR on a Bruker AC200 and Bruker MX400 WB instruments (CIGS, University of Modena e Reggio Emilia). Two dimensional NMR techniques (heteronuclear single quantum coherence and heteronuclear multiple bond correlation) were used to aid the assignment of signals in ^{1}H spectra. Compound numbering for ^{1}H NMR peaks assignment is reported in Supporting Information (Table S2). Spectra were recorded in DMSO-d_6 or $CDCl_3$. Chemicals shifts are reported in ppm from tetramethylsilane as an internal standard. When peak multiplicities are given, the following abbreviations are used: s, singlet; d, doublet; t, triplet; q, quartet; m, multiplet; br, broadened signal. Mass spectra were determined on a Finnigan MAT SSQ 710A mass spectrometer (CIGS, University of Modena and Reggio Emilia).

Of the 47 expected compounds of libraries A and B (24 and 23 molecules respectively), only 26 compounds were successfully obtained (16 and 10 molecules, respectively). The other selected fragments did not react well, affording complex mixture of undesired products.

2,4-Dimethyl-1*H*-isoindole-1,3(2*H*)-dione (10). A solution of methylamine (35%) in H_2O (1.9 mL, 22 mmol) dissolved in ethanol (20 mL) was added dropwise to a solution of 4-methyl-2-benzofuran-1,3-dione (**3**) (3 g, 18 mmol) in toluene (25 mL), and the mixture was heated at 80 °C for 4 h. After evaporation of the solvent, the oil residue was extracted four times with diethyl ether. Yield 1.52 g, 47%. ^{1}H NMR ($CDCl_3$) δ 2.71 (s, 3H, H-4), 3.16 (s, 3H, H-5), 7.45 (d, 1H, J = 7.6 Hz, H-3), 7.56 (t, 1H, J = 7.6 Hz, H-2), 7.59 (d, 1H, J = 7.6 Hz, H-1). Anal. Calcd for $C_{10}H_9NO_2$: C, 68.56; H, 5.18; N, 8.00. Found: C, 68.94; H, 5.21; N 7.77.

4-(Bromomethyl)-2-methyl-1*H*-isoindole-1,3(2*H*)-dione (11). *N*-Bromosuccinimide (1.52 g, 8.6 mmol) was added to a solution of **10** (1.5 g, 8.6 mmol) in CCl_4 (20 mL). The mixture was refluxed and irradiated with an UV lamp, and then the catalyst benzoyl peroxide (0.208 g, 0.86 mmol) in 6 mL of CCl_4 was added. The mixture was cooled with ice, and the resulting precipitate was removed by filtration. The filtrate was concentrated in vacuum, and the oil residue was crystallized several times with CH_2Cl_2/*n*-hexane, affording the product as a white solid. Yield 1.39 g, 64%; mp 138−140 °C. MS (M + H$^+$) m/z 254. ^{1}H NMR ($CDCl_3$) δ 3.19 (s, 3H, H-5), 4.99 (s, 2H, H-4), 7.70 (d, 1H, J = 6.4 Hz, H-1), 7.75 (t, 1H, J = 6.4 Hz, H-2), 7.80 (d, 1H, J = 6.4 Hz, H-3). Anal. Calcd for $C_{10}H_8BrNO_2$: C, 47.27; H, 3.17; N, 5.51. Found: C, 46.94; H, 3.20; N, 5.46.

General Synthetic Method 1 for Library A Compounds 1A, 4A, 6A, 11−12A, 15A, 18−19A, 21−23A. The appropriate ammine (0.37 mmol) in ethanol (2 mL) was added dropwise to a solution of 4-methyl-2-benzofuran-1,3-dione (**3**) (0.05 g, 0.31 mmol) in toluene (2 mL), and the reaction mixture was refluxed for 15 h. The solvent was removed under reduced pressure, and the residue was washed with ethanol (3 × 2 mL).

*5-(4-Methyl-1,3-dioxo-1,3-dihydro-2H-isoindol-2-yl)benzene-1,3-dicarboxylic Acid (**1A**).* Compound **1A** was synthesized in a similar manner to the method 1 from 5-amino-isophthalic acid, and it was isolated as a beige solid; mp 250−254 °C. ^{1}H NMR (DMSO-d_6) δ 2.68 (s, 3H, H-4), 7.70 (m, 1H, H-2), 7.78 (m, 2H, H-1 and H-3), 8.27 (t, 1H, J = 1.6 Hz, H-6), 8.49 (d, 2H, J = 1.6 Hz, H-5 and H-7), 12.95 (br, 2H, H-8). Anal. Calcd for $C_{17}H_{11}NO_6$: C, 62.77; H, 3.41; N, 4.31. Found: C, 62.90; H, 3.40; N, 4.29.

*4-Methyl-2-(2-thiophen-2-ylethyl)-1H-isoindole-1,3(2H)-dione (**4A**).* Compound **4A** was synthesized in a similar manner to the method 1 from 2-thiophen-2-ethylamine. The reaction was heated at 90 °C for 5 h. After the evaporation of the solvent, the crude residue was crystallized from methanol/H_2O, affording the white solid product; mp 58−60 °C. MS (M + H$^+$) m/z 272. ^{1}H NMR ($CDCl_3$) δ 2.70 (s, 3H, H-4), 3.23 (t, 2H, J = 5.8 Hz, H-6), 3.96 (t, 2H, J = 5.8 Hz, H-5), 6.91 (m, 2H, H-7 and H-8), 7.15 (m, 1H, H-9), 7.46 (d, 1H, J = 7.8 Hz, H-3), 7.58 (t, 1H, J = 7.8 Hz, H-2), 7.69 (d, 1H, J = 7.8 Hz, H-1). Anal. Calcd for $C_{15}H_{13}NO_2S$: C, 66.40; H, 4.83; N, 5.16. Found: C, 66.28; H, 4.92; N, 4.99.

*2-(2-Chloropyridin-4-yl)-4-methyl-1H-isoindole-1,3(2H)-dione (**6A**).* Compound **6A** was synthesized in a similar manner to the method 1 from 4-amino-2-chloropyridine. The reaction was heated at 80 °C for 16 h. After the evaporation of the solvent, the residue was treated with diethyl ether and cooled. The precipitate, the unreacted anhydride, was filtered off while the filtrate was concentrated and the residue was washed with diethyl ether, affording the beige solid product; mp 155 °C. MS (M + H$^+$) m/z 273. ^{1}H NMR ($CDCl_3$) δ 2.78 (s, 3H, H-4), 7.61 (dd, 1H, J = 5.4, 1.8 Hz, H-7), 7.67 (d, 1H, J = 6.6 Hz, H-3), 7.70 (t, 1H, J = 6.6 Hz, H-2), 7.75 (d, 1H, J = 1.8 Hz, H-5), 7.83 (d, 1H, J = 6.6 Hz, H-1), 8.51 (d, 1H, J = 5.4 Hz, H-6). Anal. Calcd for $C_{14}H_9ClN_2O_2$: C, 61.66; H, 3.33; N 10.27. Found: C, 61.27; H, 3.08; N, 10.14.

*2-[4-(1H-Imidazol-1-yl)phenyl]-4-methyl-1H-isoindole-1,3(2H)-dione (**11A**).* Compound **11A** was synthesized in a similar manner to the method 1 from 4-(1*H*-imidazol-1-yl)aniline, and it was isolated as a beige solid. mp 279−280 °C. ^{1}H NMR (DMSO-d_6) δ 2.68 (s, 3H, H-4), 7.13 (s, 1H, H-10), 7.58 (d, 2H, J = 9.0 Hz, H-6 and H-7), 7.70 (t, 1H, J = 6.3 Hz, H-2), 7.78 (m, 2H, H-1 and H-3), 7.79 (s, 1H, H-9), 7.80 (d, 2H, J = 9.0 Hz, H-5 and H-8), 8.30 (s, 1H, H-11). Anal. Calcd for $C_{18}H_{13}N_3O_2$: C, 71.28; H, 4.32; N, 13.85. Found: C, 71.15; H, 4.31; N, 13.82.

*2-(4-Hydroxybiphenyl-3-yl)-4-methyl-1H-isoindole-1,3(2H)-dione (**12A**).* Compound **12A** was synthesized in a similar manner to the method 1 from 3-aminobiphenyl-4-ol dissolved in a solution ethanol/methanol 1:1. The reaction was heated at 80 °C for 2 h. The brown solid product was washed with diethyl ether; mp 160−165 °C. MS (M + H$^+$) m/z 330. ^{1}H NMR ($CDCl_3$) δ 2.78 (s, 3H, H-4), 5.92 (br, 1H, H-13), 7.18 (d, 1H, J = 8.2 Hz, H-5), 7.27 (s, 1H, H-7), 7.32−7.46 (m, 2H, H-6 and H-10), 7.55−7.59 (m, 4H, H-8, H-9, H-11 and H-12), 7.55 (d, 1H, J = 7.4 Hz, H-3), 7.68 (t, 1H, J = 7.4 Hz, H-2), 7.82 (d, 1H, J = 7.4 Hz, H-1). Anal. Calcd for $C_{21}H_{15}NO_3$: C, 76.58; H, 4.59; N, 4.25. Found: C, 76.60; H, 4.50; N, 4.00.

*4-Methyl-2-(1,3-thiazol-2-yl)-1H-isoindole-1,3(2H)-dione (**15A**).* Compound **15A** was synthesized in a similar manner to the method 1 from 2-aminothiazol, and it was isolated as a beige solid; mp 96−99 °C. ^{1}H NMR ($CDCl_3$) δ 2.78 (s, 3H, H-4), 7.32 (s, 1H, H-6), 7.68 (d, 1H, J = 7.4 Hz, H-3), 7.69 (t, 1H, J = 7.4 Hz, H-2), 7.81 (s, 1H, H-5), 7.83 (d, 1H, J = 7.4 Hz, H-1). Anal. Calcd for $C_{12}H_8N_2O_2S$: C, 59.00; H, 3.30; N, 11.47. Found: C, 58.83; H, 3.31; N, 11.49.

*2-(3-Hydroxyphenyl)-4-methyl-1H-isoindole-1,3(2H)-dione (**18A**).* Compound **18A** was synthesized in a similar manner to the method 1 from 3-aminophenol, and it was isolated as a beige solid; mp 195−197 °C. ^{1}H NMR (DMSO-d_6) δ 2.65 (s, 3H, H-4), 6.82 (m, 3H, H-5, H-6 and H8), 7.29 (m, 1H, H-7), 7.68 (t, 1H, J = 7.2 Hz, H-2), 7.74 (m, 2H, H-1 and H-3), 9.68 (br, 1H, H-9). Anal. Calcd for $C_{15}H_{11}NO_3$: C, 71.14; H, 4.38; N, 5.53. Found: C, 70.90; H, 4.38; N, 5.51.

*3-(4-Methyl-1,3-dioxo-1,3-dihydro-2H-isoindol-2-yl)benzoic acid (**19A**).* Compound **19A** was synthesized in a similar manner to the method 1 from 3-aminobenzoic acid. The product was isolated as an oil. ^{1}H NMR (DMSO-d_6) δ 2.67 (s, 3H, H-4), 7.65 (t, 1H, J = 7.4 Hz, H-2), 7.76 (m, 2H, H-1 and H-3), 7.77 (m, 2H, H-6 and H-7), 7.99 (d, 1H, J = 7.5 Hz, H-8), 8.35 (s, 1H, H-5), 13.00 (br, 1H, H-9). Anal. Calcd for

$C_{16}H_{11}NO_4$: C, 68.32; H, 3.94; N, 4.98. Found: C, 68.45; H, 3.93; N, 4.96.

*2-(1H-Indol-4-yl)-4-methyl-1H-isoindole-1,3(2H)-dione (**21A**).* Compound **21A** was synthesized in a similar manner to the method 1 from 4-aminoindole. The product was isolated as a black solid; mp 266−270 °C. ^{1}H NMR (DMSO-d_6) δ 2.67 (s, 3H, H-4), 6.25 (d, 1H, J = 5.4 Hz, H-8), 6.99 (d, 1H, J = 7.2 Hz, H-7), 7.19 (t, 1H, J = 7.2 Hz, H-6), 7.36 (d, 1H, J = 5.4 Hz, H-9), 7.50 (d, 1H, J = 7.2 Hz, H-5), 7.69 (t, 1H, J = 7.4 Hz, H-2), 7.78 (m, 2H, H-1 and H-3), 11.31 (br, 1H, H-10). Anal. Calcd for $C_{17}H_{12}N_2O_2$: C, 73.90; H, 4.38; N, 10.14. Found: C, 74.11; H, 4.37; N, 10.13.

*2-[4-(5-Chloro-1,3-dioxo-1,3-dihydro-2H-isoindol-2-yl)-3-methylphenyl]-4-methyl-1H-isoindole-1,3(2H)-dione (**22A**).* Compound **22A** was synthesized in a similar manner to the method 1 from 2-(4-amino-2-methylphenyl)-5-chloro-1*H*-isoindole-1,3(2*H*)-dione. The reaction was heated at 90 °C. After 24 h, 2 mL of acetic acid were added and the mixture was heated at 110 °C for other 4 h. The product was isolated through filtration as a white solid; mp 274−276 °C. MS (M + H$^+$) m/z 431. ^{1}H NMR ($CDCl_3$) δ 2.27 (s, 3H, H-8), 2.78 (s, 3H, H-4), 7.33 (d, 1H, J = 8.4 Hz, H-7), 7.43 (d, 1H, J = 8.0 Hz, H-9), 7.51 (s, 1H, H-5), 7.53 (d, 1H, J = 7.6 Hz, H-3), 7.67 (t, 1H, J = 7.5 Hz, H-2), 7.78 (d, 1H, J = 8.4 Hz, H-6), 7.82 (d, 1H, J = 7.6 Hz, H-1), 7.90 (s, 1H, H-11), 7.94 (m, 1H, H-10). Anal. Calcd for $C_{24}H_{15}ClN_2O_4$: C, 66.91; H, 3.51; N, 6.50. Found: C, 66.69; H, 3.73; N, 6.43.

*2-(4-Acetylphenyl)-4-methyl-1H-isoindole-1,3(2H)-dione (**23A**).* Compound **23A** was synthesized in a similar manner to the method 1 from 4′-aminoacetophenone, and it was isolated as a white solid; mp 201−203 °C. ^{1}H NMR ($CDCl_3$) δ 2.65 (s, 3H, H-4), 2.77 (s, 3H, H-9), 7.56 (d, 1H, J = 7.6 Hz, H-3), 7.63 (d, 2H, J = 8.8 Hz, H-5 and H-8), 7.67 (t, 1H, J = 7.6 Hz, H-2), 7.81 (d, 1H, J = 7.6 Hz, H-1), 8.10 (d, 2H, J = 8.8 Hz, H-6 and H-7). Anal. Calcd for $C_{17}H_{13}NO_3$: C, 73.11; H, 4.69; N, 5.02. Found: C, 73.23; H, 4.70; N, 5.00.

General Synthetic Method 2 for Library A Compounds 5A, 8A, 17A, 20A, and 24A. A mixture of amine (6.2 mmol) and **3** (1 g, 6.2 mmol) in acetic acid (10 mL) was stirred and refluxed for 5 h; the product was precipitated by addition of water to the cooled solution. The solid was filtrated and washed with water.

*4-Methyl-2-[4-(trifluoromethyl)phenyl]-1H-isoindole-1,3(2H)-dione (**5A**).* Compound **5A** was synthesized in a similar manner to the method 2 from 4-(trifluoromethyl)aniline and it was isolated as a white solid; mp 151−153 °C. MS (M + H$^+$) m/z 306. ^{1}H NMR ($CDCl_3$) δ 2.77 (s, 3H, H-4), 7.57 (d, 1H, J = 7.6 Hz, H-3), 7.62 (t, 1H, J = 7.6 Hz, H-2), 7.67 (d, 1H, J = 7.6 Hz, H-1), 7.74 (d, 2H, J = 8.0 Hz, H-6 and H-7), 7.82 (d, 2H, J = 8.0 Hz, H-5 and H-8). Anal. Calcd for $C_{16}H_{10}F_3NO_2$: C, 62.96; H, 3.30; N, 4.59. Found: C, 63.00; H, 3.12; N 4.78.

*4-(4-Methyl-1,3-dioxo-1,3-dihydro-2H-isoindol-2-yl)benzonitrile (**8A**).* Compound **8A** was synthesized in a similar manner to the method 2 from 4-aminobenzonitrile, and it was isolated as a white solid; mp 245−250 °C. MS (M + H$^+$) m/z 263. ^{1}H NMR ($CDCl_3$) δ 2.77 (s, 3H, H-4), 7.58 (d, 1H, J = 7.2 Hz, H-3), 7.69 (t, 1H, J = 7.2 Hz, H-2), 7.70 (d, 2H, J = 9.0 Hz, H-5 and H-8), 7.81 (d, 1H, J = 7.2 Hz, H-1), 7.82 (d, 2H, J = 9.0 Hz, H-6 and H-7). Anal. Calcd for $C_{16}H_{10}N_2O_2$: C, 73.27; H, 3.64; N, 10.68. Found: C, 73.22; H, 3.45; N, 10.79.

*({[4-(4-Methyl-1,3-dioxo-1,3-dihydro-2H-isoindol-2-yl)phenyl]-carbonyl}amino)acetic Acid (**17A**).* Compound **17A** was synthesized in a similar manner to the method 2 from {[(4-aminophenyl)carbonyl]-amino}acetic acid, and it was isolated as a beige solid; mp 211−213 °C. MS (M + H$^+$) m/z 339. ^{1}H NMR (DMSO-d_6) δ 2.67 (s, 3H, H-4), 3.96 (s, 2H, H-10), 7.57 (d, 2H, J = 8.6 Hz, H-5 and H-8), 7.70 (t, 1H, J = 7.6 Hz, H-2), 7.78 (m, 2H, H-1 and H-3), 7.99 (d, 2H, J = 8.6 Hz, H-6 and H-7), 8.91 (br, 1H, H-9), 12.42 (br, 1H, H-11). Anal. Calcd for $C_{18}H_{14}N_2O_5$: C, 63.90; H, 4.17; N, 8.28. Found: C, 64.21; H, 4.02; N, 8.58.

*2-Hydroxy-4-(4-methyl-1,3-dioxo-1,3-dihydro-2H-isoindol-2-yl)-benzoic Acid (**20A**).* Compound **20A** was synthesized in a similar manner to the method 2 from 4-amino-2-hydroxybenzoic acid, and it was isolated as a beige solid; mp 289−291 °C. MS (M + H$^+$) m/z 298. ^{1}H NMR (DMSO-d_6) δ 2.66 (s, 3H, H-4), 7.37 (d, 1H, J = 8.2 Hz, H-6), 7.48 (dd, 1H, J = 8.2, 1.6 Hz, H-7), 7.55 (d, 1H, J = 1.6 Hz, H-5), 7.69 (t, 1H, J = 7.3 Hz, H-2), 7.77 (m, 2H, H-1 and H-3), 10.23 (br, 1H, H-8), 13.0 (br, 1H, H-9). Anal. Calcd for $C_{16}H_{11}NO_5$: C, 64.65; H, 3.73; N, 4.71. Found: C, 64.59; H, 3.99; N, 4.87.

*4-(4-Methyl-1,3-dioxo-1,3-dihydro-2H-isoindol-2-yl)benzenecarboximidamide Hydrochloride (**24A**).* Compound **24A** was synthesized in a similar manner to the method 2 from 4-aminobenzenecarboximidamide hydrochloride. The reaction was refluxed for 20 h. The mixture was cooled, and the formed precipitate was filtered off. The filtrate was evaporated, and the residue was triturated with acetone, affording the beige solid product; mp 234−235 °C. MS (M − Cl)$^+$ m/z 280. ^{1}H NMR (DMSO-d_6) δ 2.68 (s, 3H, H-4), 7.71 (d, 2H, J = 8.8 Hz, H-5 and H-8), 7.73 (t, 1H, J = 7.6 Hz, H-2), 7.79 (m, 2H, H-1 and H-3), 7.96 (d, 2H, J = 8.8 Hz, H-6 and H-7), 9.30 (br, 3H, H-9). Anal. Calcd for $C_{16}H_{14}ClN_3O_2$: C, 60.86; H, 4.47; N, 15.49. Found: C, 60.74; H, 4.75; N, 15.13.

General Synthetic Method 3 for Library B Compounds. A mixture of **11** (0.05 g, 0.19 mmol) in DMF (2 mL) and an opportune amine (0.3 mmol) in DMF (1 mL) was heated at 75 °C for 15 h. Then 5 mL of H_2O were added to the cooled solution.

*6-{[(2-Methyl-1,3-dioxo-2,3-dihydro-1H-isoindol-4-yl)methyl]amino}-pyridine-3-carboxylic Acid (**3B**).* Compound **3B** was synthesized in a similar manner to the method 3 from 5-aminopyridine-2-carboxylic acid, and it was isolated as a beige solid; mp 240−245 °C. ^{1}H NMR (DMSO-d_6) δ 3.09 (s, 3H, H-5), 5.96 (s, 2H, H-4), 7.16 (d, 1H, J = 9.2 Hz, H-8), 7.80 (m, 3H, H-1, H-2 and H-3), 8.28 (d, 1H, J = 9.2 Hz, H-7), 8.80 (s, 1H, H-6). Anal. Calcd for $C_{15}H_{11}N_3O_4$: C, 60.61; H, 3.73; N, 14.14. Found: C, 60.45; H, 3.72; N, 14.11.

*Ethyl 4-{[(2-Methyl-1,3-dioxo-2,3-dihydro-1H-isoindol-4-yl)methyl]-amino}benzoate (**4B**).* Compound **4B** was synthesized in a similar manner to the method 3 from benzocaine, and it was isolated as a white solid; mp 198−201 °C. ^{1}H NMR ($CDCl_3$) δ 1.38 (t, 3H, J = 7.1 Hz, H-11), 3.21 (s, 3H, H-5), 4.34 (q, 2H, J = 7.1 Hz, H-10), 4.96 (s, 2H, H-4), 6.66 (d, 2H, J = 9.0 Hz, H-6 and H-9), 7.66 (m, 2H, H-1 and H-3), 7.78 (t, 1H, J = 7.4 Hz, H-2), 7.86 (d, 2H, J = 9.0 Hz, H-7 and H-8). Anal. Calcd for $C_{17}H_{15}N_3O_4$: C, 62.76; H, 4.65; N, 12.92. Found: C, 62.62; H, 4.64; N, 12.96.

*4-{[(3-Methoxypropyl)amino]methyl}-2-methyl-1H-isoindole-1,3(2H)-dione (**7B**).* Compound **7B** was synthesized in a similar manner to the method 3 from 3-methoxypropylamine, and it was isolated as a beige solid; mp 170−175 °C. ^{1}H NMR ($CDCl_3$) δ 1.62 (m, 2H, H-8), 2.55 (m, 2H, H-7), 3.19 (s, 3H, H-5), 3.22 (s, 3H, H-10), 3.41 (t, 2H, J = 7.1 Hz, H-9), 4.20 (s, 2H, H-4), 7.78 (m, 3H, H-1, H-2 and H-3). Anal. Calcd for $C_{13}H_{16}N_2O_3$: C, 62.89; H, 6.50; N, 11.28. Found: C, 63.01; H, 6.49; N, 11.27.

*2-Methyl-4-{[(2-thiophen-2-ylethyl)amino]methyl}-1H-isoindole-1,3(2H)-dione (**9B**).* Compound **9B** was synthesized in a similar manner to the method 3 from 2-thiopheneethylamine, and it was isolated as a beige solid; mp 150−155 °C. ^{1}H NMR ($CDCl_3$) δ 3.19 (s, 3H, H-5), 3.10 (t, 2H, J = 7.4 Hz, H-8), 3.34 (m, 2H, H-7), 4.61 (br, 2H, H-4), 6.91 (m, 2H, H-9 and H-10), 7.18 (m, 1H, H-11), 7.68 (m, 2H, H-1 and H-3), 7.80 (t, 1H, J = 7.6 Hz, H-2). Anal. Calcd for $C_{15}H_{14}N_2O_2S$: C, 62.92; H, 4.93; N, 9.78. Found: C, 62.74; H, 4.94; N, 9.75.

*4-{[(2-Methyl-1,3-dioxo-2,3-dihydro-1H-isoindol-4-yl)methyl]-amino}benzenesulfonic Acid (**11B**).* Compound **11B** was synthesized in a similar manner to the method 3 from sulfanilic acid, and it was isolated as a beige solid; mp 90−95 °C. ^{1}H NMR (DMSO-d_6) δ 3.05 (s, 3H, H-5), 4.95 (s, 2H, H-4), 6.45 (d, 2H, J = 8.8 Hz, H-6 and H-7), 7.28 (d, 2H, J = 8.8 Hz, H-8 and H-9), 7.74 (m, 2H, H-1 and H-3), 7.78 (t, 1H, J = 7.6 Hz, H-2). Anal. Calcd for $C_{15}H_{12}N_2O_5S$: C, 54.21; H, 3.64; N, 8.43. Found: C, 54.33; H, 3.65; N, 8.41.

*2-Methyl-4-({[4-(phenylcarbonyl)phenyl]amino}methyl)-1H-isoindole-1,3(2H)-dione (**13B**).* Compound **13B** was synthesized in a similar manner to the method 3 from 4-aminobenzophenone, and it was isolated as a beige solid; mp 109−115 °C. ^{1}H NMR ($CDCl_3$) δ 3.20 (s, 3H, H-5), 4.89 (s, 2H, H-4), 6.75 (d, 2H, J = 8.8 Hz, H-6 and H-8), 7.31 (m, 3H, H-11, H-12 and H-13), 7.66 (m, 2H, H-1 and H-3), 7.50 (d, 2H, J = 8.8 Hz, H-7 and H-9), 7.70 (m, 2H, H-10 and H-14), 7.78 (t, 1H, J = 7.6 Hz, H-2). Anal. Calcd for $C_{22}H_{16}N_2O_3$: C, 74.15; H, 4.53; N, 7.86. Found: C, 74.29; H, 4.55; N, 7.84.

*4-{[(2-Methyl-1,3-dioxo-2,3-dihydro-1H-isoindol-4-yl)methyl]amino}-benzonitrile (**15B**).* Compound **15B** was synthesized in a similar manner to the method 3 from 4-aminobenzonitrile, and it was isolated as a white solid; mp 179−188 °C. ^{1}H NMR ($CDCl_3$) δ 3.20 (s, 3H, H-5), 4.81 (s, 2H, H-4), 6.61 (d, 2H, J = 8.4 Hz, H-6 and H-9), 7.40 (d, 2H, J = 8.4 Hz, H-7 and H-8), 7.66 (m, 2H, H-1 and H-3), 7.78 (t, 1H, J = 7.3 Hz, H-2). Anal. Calcd for $C_{16}H_{11}N_3O_2$: C, 69.31; H, 4.00; N, 15.15. Found: C, 69.25; H, 3.99; N, 15.13.

*2-Methyl-4-{[(4-nitronaphthalen-1-yl)amino]methyl}-1H-isoindole-1,3(2H)-dione (**16B**).* Compound **16B** was synthesized in a similar manner to the method 3 from 4-nitro-1-naphthylamine, and it was isolated as a brown solid; mp 160−163 °C. ^{1}H NMR ($CDCl_3$) δ 3.19 (s, 3H, H-5), 5.03 (s, 2H, H-4), 6.70 (d, 1H, J = 8.4 Hz, H-6), 7.59 (m, 4H, H-8, H-9, H-10 and H-11), 7.74 (m, 2H, H-1 and H-3), 7.82 (t, 1H, J = 7.5 Hz, H-2), 8.39 (d, 1H, J = 8.4 Hz, H-7). Anal. Calcd for $C_{19}H_{13}N_3O_4$: C, 65.70; H, 3.77; N, 12.10. Found: C, 65.76; H, 3.76; N, 12.12.

*(2-{[(2-Methyl-1,3-dioxo-2,3-dihydro-1H-isoindol-4-yl)methyl]-amino}ethyl)phosphonic Acid (**22B**).* Compound **22B** was synthesized in a similar manner to the method 3 from 2-aminoethylphosphonic acid, and it was isolated as a beige solid; mp 110−113 °C. ^{1}H NMR (DMSO-d_6) δ 2.54 (m, 4H, H-7 and H-8), 3.04 (s, 3H, H-5), 4.95 (s, 2H, H-4), 7.71 (d, 1H, J = 7.4 Hz, H-3), 7.79 (t, 1H, J = 7.4 Hz, H-2), 7.90 (d, 1H, J = 7.4 Hz, H-1), 8.13 (br, 1H, H-6). Anal. Calcd for $C_{11}H_{13}N_2O_5P$: C, 46.49; H, 4.61; N, 9.86. Found: C, 46.43; H, 4.62; N, 9.89.

*3-{[(2-Methyl-1,3-dioxo-2,3-dihydro-1H-isoindol-4-yl) methyl]amino} benzenesulfonamide (**23B**).* Compound **23B** was synthesized in a similar manner to the method 3 from 3-aminobenzenesulfonamide, and it was isolated as a white solid; mp 230−235 °C. ^{1}H NMR (DMSO-d_6) δ 3.06 (s, 3H, H-5), 4.77 (s, 2H, H-4), 6.71 (d, 1H, J = 7.2 Hz, H-6), 6.81 (br, H-10), 6.99 (d, 1H, J = 7.2 Hz, H-8), 7.06 (s, 1H, H-9), 7.16 (br, 2H, H-11), 7.21 (t, 1H, J = 7.2 Hz, H-7), 7.71 (m, 3H, H-1, H-2 and H-3). Anal. Calcd for $C_{15}H_{13}N_3O_4S$: C, 54.37; H, 3.95; N, 12.68. Found: C, 54.34; H, 3.94; N, 12.65.

Enzymology. The compounds were screened for their activity and their species-specificity against EcTS, EfTS, and hTS. Because crystallographic studies were performed also against LcTS, the activity of these compounds toward LcTS enzyme was assayed as well. LcTS, EcTS, and hTS were purified as described.[19−21] EfTS was purified following the procedure used for EcTS. The EfTS strain was a gift of Prof. Robert M. Stroud, University of California San Francisco (CA, USA). Enzyme kinetics experiments were conducted by chromogenic assay under standard conditions.[22] The K_m values, by curve-fitting to hyperbolic curves, of EcTS, EfTS, LcTS, and hTS for MTHF were, respectively, 5.8, 13.6, 5.7, and 6.9 μM. The K_i ± standard errors were determined from the nonlinear regression analysis of data from at least two independent experiments performed in triplicate.

The inhibition patterns for all the compounds were determined by steady-state kinetic analysis of the dependence of enzyme activity on MTHF concentration at varying inhibitor concentrations. All the compounds showed competitive inhibition with respect to MTHF. The apparent inhibition constant (K_i app, simply defined as K_i within the text) values were obtained from the linear least-squares fit of the residual activity as a function of inhibitor concentration, using suitable equations for competitive inhibition.[23] In the inhibition assays, the reaction mixture was the same as in the TS standard assay. Stock solutions of each inhibitor were freshly prepared in DMSO and stored at −80 °C. In the reaction mixture, the concentration of DMSO never exceeded 5%; the effect of increasing DMSO concentration in the TS assay mixture was studied, and it was observed that no change in TS activity was seen at concentrations up to 8% DMSO.[24] To obtain K_i values, the inhibitors were tested at concentrations ranging from 5 to 500 μM depending on the solubility of the compound studied. When the inhibition of hTS was studied, the concentration of the inhibitor was tested up to 50 μM.

Crystallization of Thymidylate Synthase Complexes. Crystals of LcTS complexes were grown over a few days using the sitting/hanging drop vapor diffusion technique at 20 °C from a 4 mg/mL LcTS solution (buffer: 25 mM KH_2PO_4/K_2HPO_4, pH 6.8−7.4, 1 mM EDTA) containing 40 mM dUMP. A 2 mM solution of each inhibitor in DMSO was then added in a 1:10 volume ratio to the protein/dUMP solution.[15,25,26]

In the case of complexes LcTS-dUMP−**20A** and LcTS-dUMP−**23A** complexes, drops were prepared by mixing 3 μL of the ternary complex solutions with 1 μL of precipitant solution made of 10% saturated ammonium sulfate and 1 mM DTT. The drops were then inverted over wells containing 20 mM K_2HPO_4 (pH 6.8) and 1 mM DTT. In the case of all the other complexes, drops were made by mixing equal volumes (2−3 μL) of the LcTS ternary complex solution with a precipitant solution consisting of $(NH_4)H_2PO_4/(NH_4)_2HPO_4$ 100 mM, 5% v/v PEG 400, and 20 mM Tris-HCl buffer at pH 7.4 and equilibrated against the same precipitant solution.

Crystals of the complexes appear in 5−6 days as hexagonal bipyramids and grow to the final dimensions of about 150 μm × 150 μm × 400 μm in about 2 weeks. Before the data collection, crystals were transferred to a cryoprotectant solution composed of the precipitant solution with added 30% PEG 400 and flash frozen in liquid nitrogen. The data collection and refinement statistics are reported in Table 2.

Data Collection and Structure Determination. Data sets related to LcTS-dUMP−**6A**_1, LcTS-dUMP−**8A**, LcTS-dUMP−**12A**_1 complexes were collected using synchrotron radiation from the European Synchrotron Radiation Facility, Grenoble, France (ESRF) ID14−1 with wavelength of 0.930 Å with the rotation technique ($\Delta\varphi$ = 1°) and an ADSC Quantum 4 detector. The data set of the LcTS-dUMP−**6A**_2 complex was collected using synchrotron radiation from the European Synchrotron Radiation Facility, Grenoble, France (ESRF) ID23−1 with wavelength of 1.008 Å, the rotation technique ($\Delta\varphi$ = 0.75°), and a MARresearch CCD 225 detector. The data set of the LcTS-dUMP−**12A**_2 complex was collected using synchrotron radiation of European Molecular Biology Laboratory (EMBL) PX beamline BW7B at the DORIS storage ring, DESY, Hamburg, Germany, with wavelength of 1.078 Å, the rotation technique ($\Delta\varphi$ = 1°), and detector MARresearch CCD 225 detector. The data sets of the LcTS-dUMP−**20A**, LcTS-dUMP−**23A**, and LcTS-dUMP−**24A** complexes were collected using synchrotron radiation from the ESRF beamline ID23−1 with wavelength of 0.983 Å, the rotation technique ($\Delta\varphi$ = 0.5°), and a ADSC Quantum Q315r detector.

All the data sets were processed using MOSFLM 6.2[27,28] and scaled with SCALA.[29]

The structure solutions of all complexes were performed by the molecular replacement method using the MOLREP software,[28,30] where one subunit of LcTS (PDB entry 1LCA) was used as a model for the rotation and translation functions. All structures were refined and water molecules were added using REFMAC[29,31] and ARP/WARP,[31] respectively.

The program Xtalview/Xfit[33] and Coot[32] were used for manual rebuilding of the molecule, modeling of the inhibitor molecules into the electron density map and visualization for all structures.

Figures were generated using CCP4MG from the CCP4 suite[28] and Chimera[34] program.

■ ASSOCIATED CONTENT

Supporting Information. Binding modes of known phthalein and naphthalein compounds (PTH; α156, MR20, GA9); designed libraries A and B; calculated molecular properties for libraries A and B; atom numbering in compounds characterized through NMR; plot of the enzyme kinetic inhibition profiles (K_i) for libraries A and B; contact distances between substrates and LcTS residues. This material is available free of charge via the Internet at http://pubs.acs.org.

Accession Codes

The X-ray coordinates of compounds **6A**, **8A**, **12A**, **20A**, **23A**, and **24A** bound to LcTS-dUMP have been deposited in the Protein Data Bank with accession numbers 3C06 (**6A**), 3C0A (**6A**), 3BNZ (**8A**), 3BYX (**12A**), 3BZ0 (**12A**), 3IK1 (**20A**), 3IJZ (**23A**), and 3IK0 (**24A**).

■ AUTHOR INFORMATION

Corresponding Author

*For M.P.C.: phone, 0039-059-205-5125; fax, 0039-059-205-5131; E-mail, mariapaola.costi@unimore.it. For S.M.: phone, 0039-0577-234255; fax, 0039-0577-234233; E-mail, mangani@unisi.it. For S.F.: phone, 0039-059-205-5331; fax, 0039-059-205-5131; E-mail, stefania.ferrari@unimore.it.

Present Addresses

[§]Roche Pharma (Schweiz) AG, Schönmattstrasse 2, 4153 Reinach (BL), Switzerland.

■ ACKNOWLEDGMENT

This work was financially supported by MIUR-PRIN 2006-2006030430_004 CSTMPL. We thank the Cassa di Risparmio di Modena (CDRM) Foundation. We are grateful to Merck Eprova AG, Switzerland, an affiliate of Merck KGaA, Darmstadt, Germany, for providing the (6*R*)-5,10-methylenetetrahydrofolic acid sodium salt. We also acknowledge ESRF and the EMBL Hamburg outstation for the use of their beamlines for data collection. We thank Professor B. K. Shoichet for providing the pdb file of the crystallographic complex LcTS-PTH, Professor Marcella Rinaldi for assistance with the synthetic work, and Fabrizia Soragni for her technical assistance.

■ ABBREVIATIONS USED

$CDCl_3$, deuterated trichloromethane; DMF, dimethylformamide; DMSO, dimethyl sulfoxide; dTMP, 2′-deoxythymidine-5′-monophosphate; DTT, dithiotreitol; dUMP, 2′-deoxyuridine-5′-monophosphate; EcTS, *Escherichia coli* thymidylate synthase; EDTA, ethylenediaminetetraacetic acid; EfTS, *Enterococcus faecalis* thymidylate synthase; hTS, human thymidylate synthase; K_i, inhibition constant; LcTS, *Lactobacillus casei* thymidylate synthase; MTHF, N^5,N^{10}-methylene tetrahydrofolate; PEG 400, polyethylene glycol, MW 400; PTH, phenolphthalein; SD, small domain; TS, thymidylate synthase

■ REFERENCES

(1) Carreras, C. W.; Santi, D. V. The catalytic mechanism and structure of thymidylate synthase. *Annu. Rev. Biochem.* **1995**, *64*, 721–762.

(2) Chu, E.; Callender, M. A.; Farrell, M. P.; Schmitz, J. C. Thymidylate synthase inhibitors as anticancer agents: from bench to bedside. *Cancer Chemother. Pharmacol.* **2003**, *52* (Suppl1), S80–S89.

(3) Shoichet, B. K; Stroud, R. M.; Santi, D. V.; Kuntz, I. D.; Perry, K. M. Structure-based discovery of inhibitors of thymidylate synthase. *Science* **1993**, *259*, 1445–1450.

(4) Finer-Moore, J. S., Blaney, J., Stroud, R. M., *Computational and Structural Approaches to Drug Discovery*; Stroud, R. M. and Finer-Moore, J. S., Eds; RSC: Cambridge, UK, 2008. p 9.

(5) Stout, T. J.; Tondi, D.; Rinaldi, M.; Barlocco, D.; Pecorari, P.; Santi, D. V.; Kuntz, I. D.; Stroud, R. M.; Shoichet, B. K.; Costi, M. P. Structure-based design of inhibitors specific for bacterial thymidylate synthase. *Biochemistry* **1999**, *38*, 1607–1617.

(6) Costi, M. P.; Rinaldi, M.; Tondi, D.; Pecorari, P.; Barlocco, D.; Ghelli, S.; Stroud, R. M.; Santi, D. V.; Stout, T. J.; Musiu, C.; Marangiu, E. M.; Pani, A.; Congiu, D.; Loi, G. A.; La Colla, P. Phthalein derivatives as a new tool for selectivity in thymidylate synthase inhibition. *J. Med. Chem.* **1999**, *42*, 2112–2124.

(7) Ghelli, S.; Rinaldi, M.; Barlocco, D.; Gelain, A.; Pecorari, P.; Tondi, D.; Rastelli, G.; Costi, M. P. *ortho*-Halogen naphthaleins as specific inhibitors of *Lactobacillus casei* thymidylate synthase. Conformational properties and biological activity. *Bioorg. Med. Chem.* **2003**, *11*, 951–963.

(8) Calò, S.; Tondi, D.; Venturelli, A.; Ferrari, S.; Pecorari, P.; Rinaldi, M.; Ghelli, S.; Costi, M. P. A step further in the discovery of phthalein derivatives as thymidylate synthase inhibitors. *ARKIVOC* **2004**, 382–396.

(9) Finer-Moore, J. S.; Anderson, A. C.; O'Neil, R. H.; Costi, M. P.; Ferrari, S.; Krucinski, J.; Stroud, R. The structure of *Cryptococcus neoformans* thymidylate synthase suggests strategies for using target dynamics for species-specific inhibition. *Acta Crystallogr., Sect. D: Biol. Crystallogr.* **2005**, *D61*, 1320–1334.

(10) Costi, M. P.; Gelain, A.; Barlocco, D.; Ghelli, S.; Soragni, F.; Raniero, F.; Rossi, T.; Ruberto, A.; Guillou, C.; Cavazzuti, A.; Casolari, C.; Ferrari, S. Anti-bacterial agent discovery using thymidylate synthase bio-library screening. *J. Med. Chem.* **2006**, *49*, 5958–5968.

(11) Babaoglu, K.; Shoichet, B. K. Deconstructing fragment-based inhibitor discovery. *Nature Chem. Biol.* **2006**, *2*, 720–723.

(12) *ChemFinder Ultra Database 7.0*; Cambridge Soft Corporation, htpp://www.cambridgesoft.com.

(13) *ACDlab 6.0 Software*; Cambridge Soft Corporation, htpp://www.cambridgesoft.com.

(14) Lipinski, C. A.; Lombardo, F.; Dominy, B. W.; Feeney, P. J. Experimental and computational approaches to estimate solubility and permeability in drug discovery and development settings. *Adv. Drug Delivery Rev.* **2001**, *46*, 3–26.

(15) Hardy, L. W.; Finer-Moore, J. S.; Montfort, W. R.; Jones, M. O; Santi, D. V.; Stroud, R. M. Atomic structure of thymidylate synthase: target for rational drug design. *Science* **1987**, *235*, 448–455.

(16) Finer-Moore, J.; Fauman, E. B.; Foster, P. G.; Perry, K. M.; Santi, D. V.; Stroud, R. Refined structures of substrate-bound and phosphate-bound thymidylate synthase from *Lactobacillus casei*. *J. Mol. Biol.* **1993**, *232*, 1101–1116.

(17) Ferrari, S.; Losasso, V.; Costi, M. P. Sequence-Based identification of specific drug target regions in the thymidylate synthase enzyme family. *ChemMedChem* **2008**, *3*, 392–401.

(18) Ferrari, S.; Costi, M. P.; Wade, R. Inhibitor specificity via protein dynamics: insights from the design of antibacterial agents targeted against thymidylate synthase. *Chem. Biol.* **2003**, *10*, 1183–1193.

(19) Kealey, J. T.; Santi, D. V. Purification methods for recombinant *Lactobacillus casei* thymidylate synthase and mutants: a general, automated procedure. *Protein Expression Purif.* **1992**, *4*, 380–385.

(20) Maley, G. F.; Maley, F. Properties of a defined mutant of *Escherichia coli* thymidylate synthase. *J. Biol. Chem.* **1988**, *263*, 7620–7627.

(21) Pedersen-Lane, J.; Maley, G. F.; Chu, E.; Maley, F. High-level expression of human thymidylate synthase. *Protein Expression Purif.* **1997**, *10*, 256–262.

(22) Pogolotti, A. L., Jr.; Danenberg, P. V.; Santi, D. V. Kinetics and mechanism of interaction of 10-propargyl-5,8-dideazafolate with thymidylate synthase. *J. Med. Chem.* **1986**, *29*, 478–482.

(23) Segel, I. H. Enzyme Kinetics. *Behaviour and Analysis of Rapid Equilibrium and Steady-State Enzyme Systems*; John Wiley and Sons: New York, 1975, p 105.

(24) Cavazzuti, A; Paglietti, G; Hunter, W. N.; Gamarro, F; Piras, S; Loriga, M; Alleca, S; Corona, P; McLuskey, K; Tolloch, L.; Gibellini, F.; Ferrari, S.; Costi, M. P. Discovery of potent pteridine reductase inhibitors ot guide antiparasite drug development. *Proc. Natl. Acad. Sci. U.S.A.* **2008**, *105*, 1448–1453.

(25) Jaspard, E. Role of protein−solvent interactions in refolding: effects of cosolvent additives on the renaturation of porcine pancreatic elastase at various pHs. *Arch. Biochem. Biophys.* **2000**, *15*, 220–228.

(26) Bhattacharjya, S.; Balaram, P. Effects of organic solvents on protein structures: observation of a structured helical core in hen egg-white lysozyme in aqueous dimethylsulfoxide. *Proteins* **1997**, *29*, 492–507.

(27) Leslie, A. G. W. *Crystallographic Computing V*; Moras, D., Podjarny, A. D., Thierry, J.-C., Eds.; Oxford University Press: Oxford, 1991; pp50−61.

(28) Collaborative Computational Project, No. 4. The CCP4 suite: programs for protein crystallography. *Acta Crystallogr., Sect. D: Biol. Crystallogr.* **1994**, *50*, 760−763.

(29) Evans, P. R. SCALA, continuous scaling program. *Joint CCP4 ESF-EACBM Newsletter* **1997**, *33*, 22−24.

(30) Vagin, A; Teplyakov, A. MOLREP: an automated program for molecular replacement. *J. Appl. Crystallogr.* **1997**, *30*, 1022–1025.

(31) Murshudov, G. N.; Vagin, A. A.; Dodson, E. J. Refinement of macromolecular structures by the maximum-likelihood method. *Acta Crystallogr., Sect. D: Biol. Crystallogr.* **1997**, *53*, 240–255.

(32) Perrakis, A.; Morris, R. J. H.; Lamzin, V. S. Automated protein model building combined with iterative structure refinement. *Nature Struct. Biol.* **1999**, *6*, 458–463.

(33) McRee, D. E. XtalView/Xfit—a versatile program for manipulating atomic coordinates and electron density. *J. Struct. Biol.* **1999**, *125*, 156–165.

(34) *UCSF Chimera, Production Version 1 Build 2038 2004/10/18*, 2004.